Materials Research. 2015; 18(5): 1044-1052
DOI: http://dx.doi.org/10.1590/1516-1439.016415

Fabrication of Cathode Materials Based on $Limn_2o_4$/Cnt and $Lini_{0.5}mn_{1.5}o_4$/Cnt Nanocomposites for Lithium – Ion Batteries Application

Thang Van Le[a,b]*, My Loan Phung Le[c], Man Van Tran[c], Nguyet Minh Thi Nguyen[b], Anh Tuan Luu[a], Ha Tran Nguyen[a,b]

[a]*Faculty of Materials Technology, Ho Chi Minh University of Technology, 268 Ly Thuong Kiet, Ward 14, District 10, Ho Chi Minh City, Viet Nam*
[b]*Materials Technology Key Laboratory, Vietnam National University Ho Chi Minh City, 268 Ly Thuong Kiet, District 10, Ho Chi Minh City, Viet Nam*
[c]*Department of Physical Chemistry, University of Science, VNU-HCM, 227 Nguyen Van Cu Street, District 5, Ho Chi Minh City, Viet Nam*

Received: July 10, 2015; Revised: August 24, 2015

Carbon nanotubes (CNTs) are a promising candidate material for use in lithium batteries due to 1D tubular structure, high electrical, thermal conductivities, and extremely large surface area. In this work, the MWCNTs were purified by dispersion in a mixture of HNO_3 and H_2SO_4 acids. The oxidized-MWCNTs were used as conducting addition to prepare a nanocomposites as high performance cathode material for Li-ion batteries (LIBs). The spinel cathode materials of $LiMn_2O_4$ (LMO), doped spinel $LiNi_{0.5}Mn_{1.5}O_4$ (LNMO) were synthesized and characterized via X-rays diffraction (XRD), scanning electron microscopy (SEM) and transmission electron microscopy (TEM). The electrochemical properties of nanocomposites based on LMO/CNTs and LMNO/CNTs were investigated by cyclic voltammetry (CV) as well as electrochemical impedance spectroscopy (EIS). The EIS measurement indicated that the LMO (LNMO)/CNTs nanocomposites showed lower charge transfer resistance (R_{ct}) than that of LMO(LNMO)/ Vulcan carbon materials. In addition, the studied nanocomposites cathodes gave a specific capacity of 145 Ah.kg^{-1} and 120 Ah.kg^{-1} for LMO/CNTs (10 wt%) and LNMO/CNTs (10 wt%), respectively, measured at a charge/discharge rate of 0.1C.

Keywords: *nanocomposites, multiwall carbon nanotubes (MWCNTs), spinel materials, lithium-ion batteries (LIBs)*

1. Introduction

The demand of higher energy density and higher power capacity of lithium (Li)-ion secondary batteries has led to the search for electrode materials whose capacities and performance are better than those available today[1-8]. Commonly, a typical LIB includes an anode made from graphite, and a positive electrode (cathode) made from $LiCoO_2$ and a Li-ion conducting electrolyte. When the cell is charged, Li ions are extracted from the cathode, pass through the electrolyte and are inserted into the anode. Upon discharging, the Li ions are released by the anode and move back to the cathode. The electrons pass around the external circuits in opposite directions. Compared to traditional rechargeable batteries such as lead acid and Ni-Cd batteries, rechargeable LIBs provide many advantages including high voltage, high energy-to-weight ratio, i.e. high energy density, long cyclic life, no memory effect and slow loss of charge[1-3]. For these advantages, LIBs are currently the most popular battery type of powering portable electronic devices. Although LIBs have shown remarkably commercial success, the electrodes and their component materials are still the target of interesting research for enhancement of electrochemical performance of batteries devices. The main disadvantages of LIBs are low power density as well as low ion diffusion and charge transfer during the process of charge–discharge at high rates as a consequence of high polarization[9-11]. Therefore, the development of new electrodes having a large surface area, a short diffusion and high electric/thermal conductions, is necessary to overcome the disadvantages of conventional materials.

Carbon nanotubes (CNTs), having high electronic conductivity, good lithium permeability and electrochemical stability, are particularly attractive for LIB applications[12-14]. The hybrid nanostructures obtained by incorporating CNTs into Li-storage compounds as novel electrode materials have been developed utilizing the aforementioned attractive properties of CNTs[15-19]. The use of CNTs in electrodes results in many advantages because of their high specific surface area as well as mechanical and transport properties. Recently, there have been many reports presenting the structures combining CNTs and nanoparticles such as V_2O_5 and SnO_2[20] via a hydrothermal process. Such obtained V_2O_5- SnO_2/CNT composites display fast Li^+ transformation and high electronic conductivity. Jiang et al.[4] has reported

*e-mail: vanthang@hcmut.edu.vn

direct-growth method by an in-situ hydrothermal to make high performance and flexible $LiMn_2O_4$/CNTs cathode without binder. The flexible cathode materials show a high capacity of and a stable cycling performance and thus have a great potential for flexible lithium ion batteries. More recently, Zhu et al.[21] has reported $CuCrO_2$–CNTs nanocomposites, which were fabricated by an in-situ hydrothermal method. This material exhibits excellent reversible specific capacity and cyclic performance. Even at high charge/discharge rates (1 C), the specific capacity retention was still as high 530 $mAhg^{-1}$ after 40 cycles. In this study, we presented the synthesis and characterization of nanocomposites based on LMO/CNTs and LMNO/CNTs materials. We also investigated the impact of CNTs contents (2-10 wt%) in their nanocomposites to electrochemical properties of cathode material in LIBs application.

2. Experimental Procedure

2.1. Material

Baytubes C150P (Bayer Material-Science AG, Germany), synthesized via the chemical vapor deposition (CVD) method, were used as received. Polytetrafluoroethylene 60 wt % dispersion in H_2O, Lithium carbonate (99%) (Li_2CO_3), Manganese dioxide (99%) (MnO_2), Manganese carbonate (99.9%) ($MnCO_3$), and Nickel(II) Nitrate Hexahydrate (99.99%) ($Ni(NO_3)_2.6H_2O$) were purchased from Sigma Aldrich. H_2SO_4 (95%) and HNO_3 (65%) were purchased from Fisher/Acros as received.

2.2. CNTs purification

150 mg of CNTs was immersed in 100 mL of the mixture of H_2SO_4 (95%) and HNO_3 (65%). The reaction was performed in sonication bath for 4 hours. The CNTs were washed with deionized (DI) water several times, then were filtered and dried until constant weight. Finally, the morphology and structure of CNTs were characterized by scanning electron microscopy (SEM), transmission electron microscope (TEM) and Fourier Transform infrared (FTIR) spectroscopy.

2.3. Synthesis of $LiMn_2O_4$ (LMO) and $LiNi_{0.5}Mn_{1.5}O_4$ (LNMO) materials

The cathode materials $LiMn_2O_4$ (LMO) and $LiNi_{0.5}Mn_{1.5}O_4$ (LNMO) were synthesized by *solid state reaction*.

Synthesis of LMO: Li_2CO_3 (2.5g, 67.6 mmol) and MnO_2 (5.8 g, 67.6 mmol) were initially mixed together and annealed at 600 °C for 24 hours. The mixture was then re-grounded, pressed into pellets and reacted repeatedly at 830 °C in air for 24 hours.

Synthesis of LNMO: Li_2CO_3 (2.5 g, 67.6 mmol), $MnCO_3$ (23.32 g, 0.202 mol), $Ni(NO_3)_2.6H_2O$ (19.65 g, 67.6 mmol) were mixed together and decomposed at 600 °C for 24 hours. Then, the mixture was re- grounded, pressed into pellets and reacted repeatedly at 900 °C for 24 hours. Finally, the material was cooled down and kept heating at 700 °C for 24 hours to obtain LNMO.

2.4. Formation of LMO (LNMO)/CNTs nanocomposites

The nanocomposites LMO (LNMO)/CNTs was prepared by mixing method in ethanol solvent. The schematic illustration of nanocomposites formation process was shown in Figure 1. The cathode composition consists of 80 wt% spinel material, 10 wt% binder of 60%wt PTFE emulsion in water and 10 wt% of conducting agents (CNTs, Vulcan carbon). The effect of CNTs on cathode performance was studied for different CNTs ratios: 2, 4, 6, 8 and 10 wt%. The electrode material was firstly mixed with conducting agents in ethanol solution by using the IKA stirrer. The mixture was stirred in 15 minutes, and the solvent was evaporated at 80°C for 15 minutes. Then, the binder was finally added to obtain the cathode paste. This paste was rolled down to 0.1 mm thickness and cut into pellets with diameter 10 mm and dried at 130°C under vacuum for 24 hours.

3. Characterization

FTIR (Thermo fisher scientific-model Nicolet 6700, frequency range of 4,000-500 cm^{-1}). Attenuated total reflection Fourier transform infrared (ATR FT-IR) spectra were recorded using BIO-RAD Excalibur spectrometer

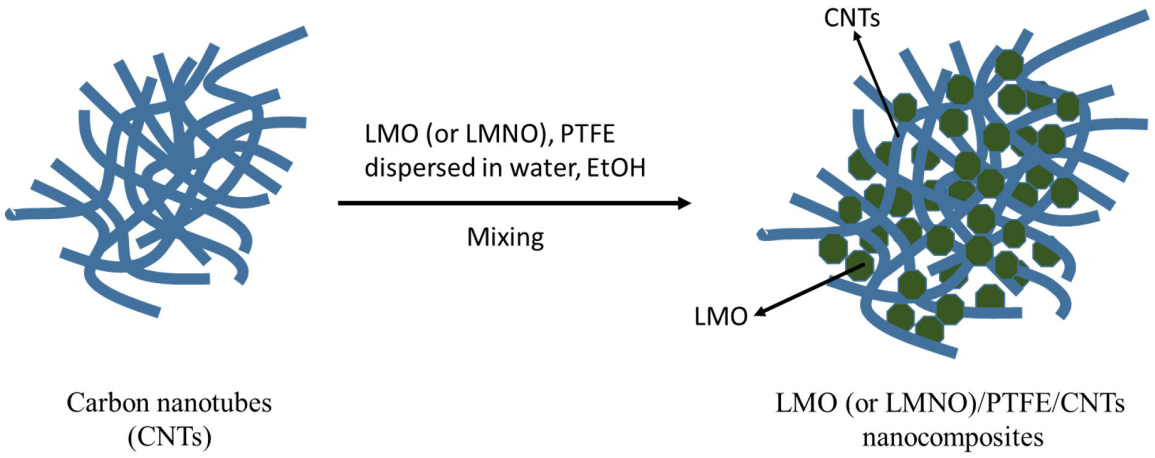

Figure 1. Schematic illustration of LMO (LNMO)/CNTs nanocomposites by mixing method.

equipped with an ATR Harrick Split PeaTM, the samples were recorded as the average of 128 scans with a resolution of 4 cm^{-1}. Wide-angle powder X-ray diffraction (XRD) patterns were recorded at room temperature on a Bruker AXS D8 Advance diffractometer using Cu-Kα radiation (k =0.15406 nm), at a scanning rate of 0.05 degrees per second. SEM images were acquired using a field-emission scanning electron microscope (NOVA NANOSEM450, FEI) equipped with an Oxford energy dispersive X-ray (EDX) analysis system. TEM images were performed on a FEI Tecnai F20 microscope equipped with an Oxford EDX analysis system and with an acceleration voltage of 200 kV.

Cyclic voltammetry (CV) was performed on MGP2 (Biologic, France) using ECLab software. The electrochemical cell including three electrode cells: a platinum electrode covered with a composite material as a working electrode (WE), an Ag/0.1 M AgNO3/0.01M TBAP in acetonitrile as reference electrode (RE) and a Pt wire as counter electrode (CE). The electrolyte solution consists of 0.75 M lithium bis(trifluoromethanesulfonyl)imide (LiTFSI) dissolved in 1:1 mixture of ethylene carbonate (EC) and dimethyl carbonate (DMC)[22-24]. The standard voltage of the reference electrode is 0.542 V versus SHE at 25 °C.

The impedance measurement (EIS) was performed in Swagelok-type batteries at room temperature. The cell consisting two electrode films as positive and negative electrodes was assembled. The electrolyte was a 1 M solution of $LiClO_4$ in EC-DMC (1:1). The EIS was carried out using an Autolab 302N (MetroOhm).

Cycling tests were performed in Swagelok-type batteries at room temperature by using Swagelok-type batteries. Positive electrode pastes were composite of LMO (LNMO)/CNT. Negative electrodes were 200 μm thick lithium foil (Sigma Aldrich). Typical active material masses used were 15 - 20 mg/cm^2. The electrolyte was a 1M solution of $LiPF_6$ in EC:DMC with the volume ratio 50:50 (Merck Co.). Cells were assembled in a glove box under argon to avoid oxygen and water. Electrochemical studies were carried out using MGP2 (Biologic, France) in the potential window 3.50 - 4.85 V vs Li/Li^+, in galvanostatic mode at C/10 – C/20 regime.

4. Results and Discussion

4.1. Structure and morphology of purified CNTs

Purified CNTs were initially treated with a mixture of H_2SO_4 (95%)/HNO_3 (65%) to clean the surface. Moreover, this treatment process also functionalized reacting groups such as hydroxyl, carboxyl, and carbonyl groups on the surface of CNTs. These functional groups not only facilitated the dispersion of the CNTs in water but also acted as centers for incorporation of metal oxide particles. The structures and morphologies of CNTs were characterized via SEM and TEM. Figure 2 showed the SEM images of CNTs before (a) and after (b) the purification process using H_2SO_4 (95%)/HNO_3 (65%). The morphology of CNTs was additionally confirmed by TEM. The TEM images of purified CNTs (Figure 3b) are much clearer comparing with the as-prepared one (Figure 3a). These results suggest that the CNTs were successfully purified using the acid treatment process.

The functional groups such as hydroxyl and carboxyl groups of CNTs were characterized via FTIR. The presence of hydroxyl groups and carbonyl groups corresponds to the appearance of broad peaks at 3425 cm^{-1} and 1736 cm^{-1}, respectively. It should be noted that the CNTs containing hydroxyl and carbonyl groups would be necessary to be easily dispersed in polar solvents

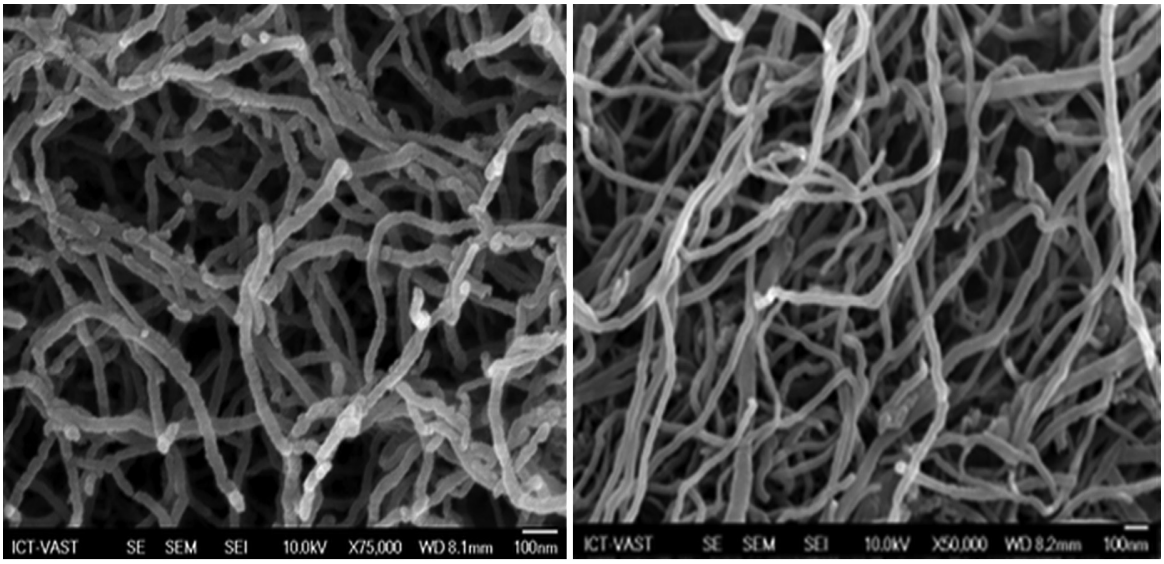

Figure 2. SEM images of CNTs before (a) and after (b) acid treatment.

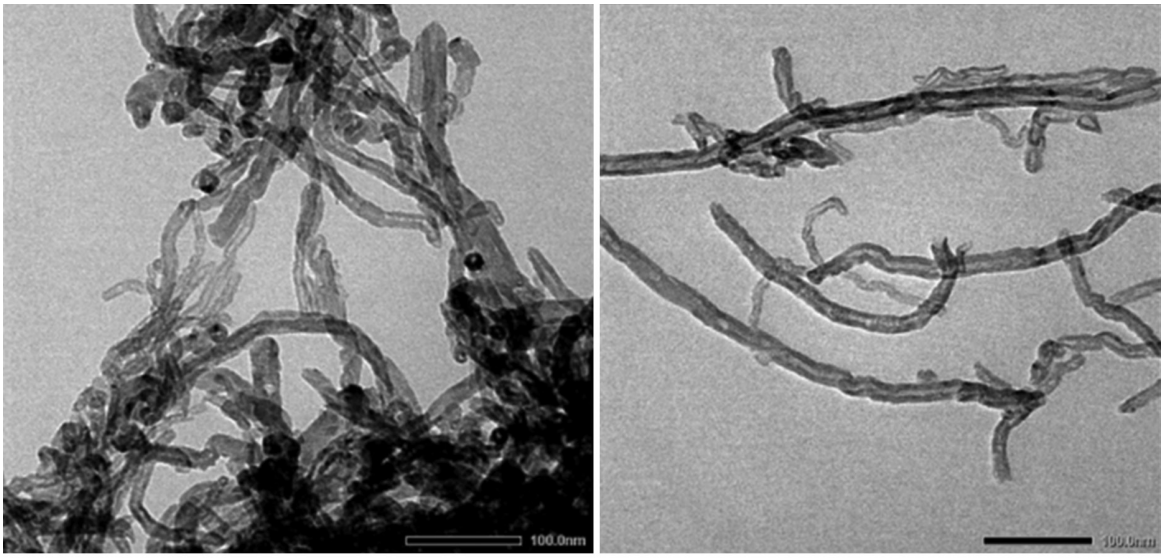

Figure 3. TEM images of CNTs before (a) and after (b) acid treatment.

4.2. Structure and morphology of $LiMn_2O_4$ (LMO) and $LiNi_{0.5}Mn_{1.5}O_4$ (LNMO)

Figure 4 shows X-ray diffraction patterns of the sample $LiMn_2O_4$ and $LiNi_{0.5}Mn_{1.5}O_4$. The XRD patterns *2θ = 18°, 36.5°, 38°, 44°, 48°, 58° and 64°* could be assigned to face center cubic phase (fcc). The obtained materials were monophasic without impurity. The morphology of particles was analyzed by SEM images (Figure 5). The LMO shows the well-faceted octahedral particles, while the morphology of the LNMO particles exhibits irregular cubes. Both LMO and LNMO particles exhibit grain sizes from 0.5 μm to 1 μm.

4.3. Structure of LMO (LNMO)/CNTs nanocomposites

The structure of LMO (LNMO)/CNTs nanocomposites was also determined by XRD. The XRD diagram in Figure 6 shows the specific peak related to CNTs at 25°, and all characteristic peaks corresponding to LMO/LNMO spinel phase at *18°, 36.5°, 38°, 44°, 48°, 58° and 64°*, respectively. The result confirms the formation of nanocomposites LMO (LNMO)/CNTs by mixing process.

The morphologies of LMO (LNMO)/CNTs nanocomposites were characterized via SEM in Figure 7. The SEM results show a 1D tubular structure of the LMO (LNMO)/CNTs composite after mixing.

A typical low-magnification transmission electron microscopy (TEM) image (Figure 8) further shows that LMO (LNMO) distributed randomly on the CNTs surface. It should be noted that the particle size distribution of LMO and LNMO is much smaller than original particle size of LMO and LNMO. This phenomenon can be explained that the preparation of LMO (LNMO)/CNTs nanocomposites via mixing process eliminated the particles aggregation. Therefore the obtained particle size distribution of LNO and LMNO in their nanocomposites is around 50 nm. These

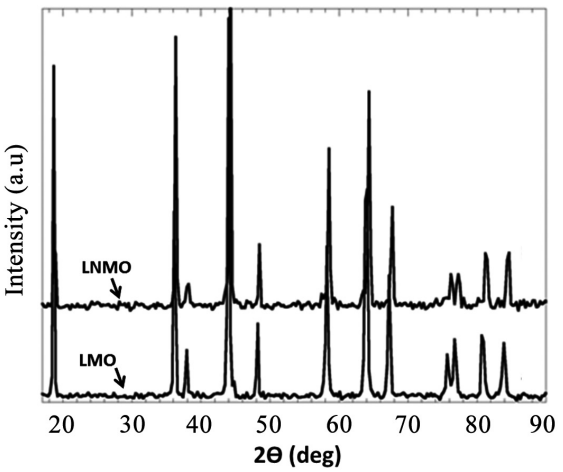

Figure 4. XRD patterns of LMO and LNMO materials.

results confirm that LMO and LNMO particles were deposited on the surface of the LMO (LNMO)/CNTs nanocomposites. More interestingly, the LMO (LNMO)/CNTs nanocomposites exhibit an interpenetrating network structure that offers a benefit of charge transfer in cathode materials.

4.4. Electrochemical properties of LMO (LNMO)/CNTs nanocomposites

Li^+ intercalation/de-intercalation in LMO/CNTs and LNMO/CNTs nanocomposites as cathode electrode materials was characterized via cyclic voltammetry (CV). Figure 9 and Figure 10 show the CV curves of LMO (LNMO)/CNTs (2 wt%) compared to LMO (LNMO)/VC (Vulcan-Carbon ~ 2 wt%) as a standard material for comparison. The CV curves were carried out with a potential region of 0.1-1.3 V vs $Ag/AgNO_3$ and a scanning rate of 0.2 mV/s in an 0.75 M LiTFSI/EC:DMC (1:1 by v/v) electrolyte solution. In the case of

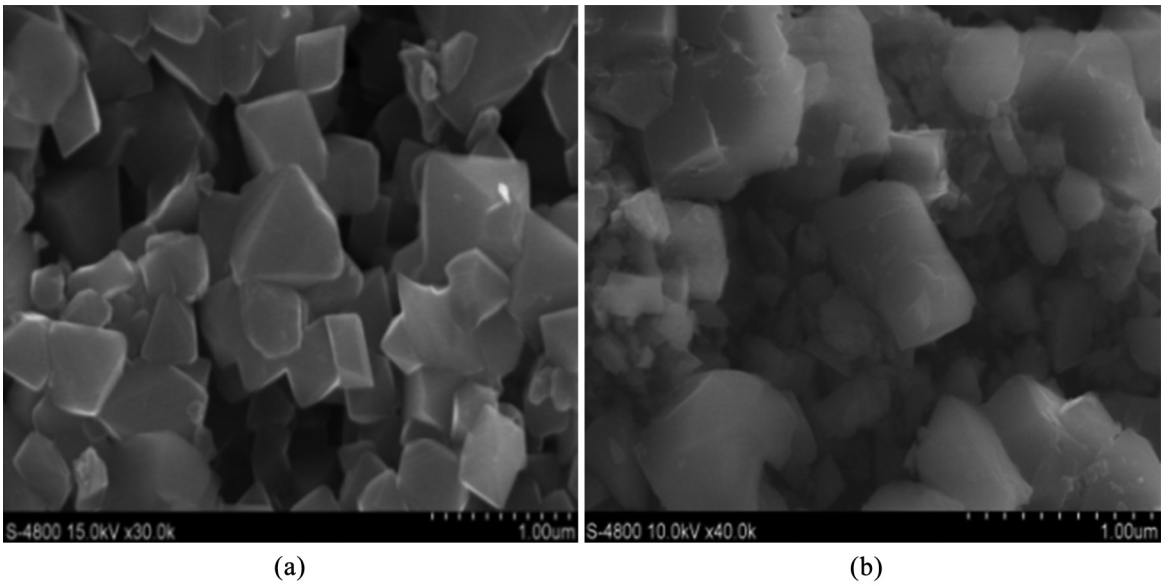

Figure 5. SEM images of LMO particles (a) and LNMO particles (b).

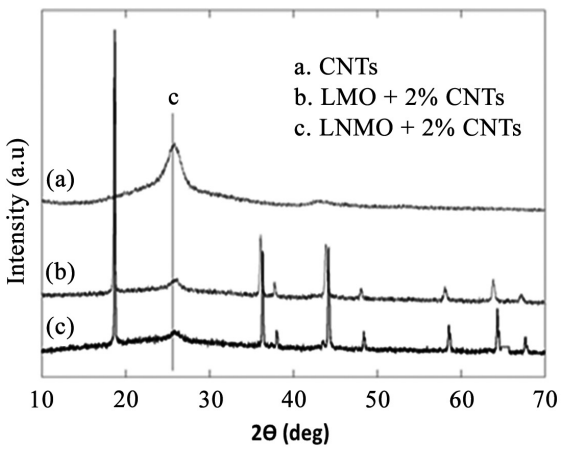

Figure 6. XRD of LMO (LNMO)/CNTs nanocomposites.

LMO/CNTs, the CV curve shows double oxidation-reduction peaks on the forward and backward scanning. As seen in Figure 8, the oxidation and reduction peaks in those curves relate to the Mn^{3+}/Mn^{4+} redox couple, indicating the lithium intercalation/de-intercalation via the oxidation-reduction process. The intensity of Mn^{3+}/Mn^{4} oxidation and reduction peaks of the LMO/CNTs nanocomposites is higher than that of the LMO/Vulcan Carbon materials. Similar to the CV results of LMO/CNTs, the intensity of Ni^{+4}/Ni^{+2} oxidation and reduction peaks in LNMO/CNTs nanocomposites is also higher than that in LMO/Vulcan Carbon materials. These results proved that the higher efficiency of LMO (LNMO)/CNTs nanocomposites is better than LMO (LMNO)/Vulcan materials. Moreover the increase of wt% CNTs in LMO(LNMO)/CNTs nanocomposites leading to enhance the intensity of Mn^{3+}/Mn^{4+} and Ni^{+4}/Ni^{+2} compared to the LMO(LNMO)/VC at the same wt% of Carbon Vulcan. The highest intensity of Mn^{3+}/Mn^{4+} and Ni^{+4}/Ni^{+2} redox couple obtained at 10 wt% of CNTs in LMO(LNMO)/CNTs nanocomposites.

The electronic conductivity of LMO/CNTs and LNMO/CNTs nanocomposites compared to LMO (LNMO)/Vulcan Carbon was characterized by electrochemical impedance spectroscopy (EIS) as shown Figure 11 and Figure 12, respectively. As seen in the Nyquist plot spectra, at a high content of Vulcan Carbon, the charge transfer resistance (R_{ct}) of LMO/Vulcan Carbon (10 wt%) decreases significantly and the diffusion resistance corresponding to Warburg (W) at low frequencies seem to dominate. On the other hand, the Warburg value of LMO (LNMO)/CNTs (10 wt%) is much lower than that of LMO (LNMO)/Vulcan Carbon (10 wt%). These results indicate that the electrochemical reaction of LMO (LNMO)/CNTs nanocomposites is better than that of LMO (LNMO)/VC as a result of high diffusion of lithium ions in the charge-discharge process.

Charge – discharge profile of the LMO (LNMO)/CNTs was characterized at the current density C/10 using Swagelok-type cell. The charge-discharge capacity of LMO/CNTs (10 wt%) exhibited the value of 145 $Ah.kg^{-1}$ that much higher than LMO/Carbon Vulcan (10 wt%) (70 $Ah.kg^{-1}$) (Figure 13). To reach more insights into the efficiency of CNTs for charge – discharge process, we measured charge – discharge capacity of LMO/CNTs (2 wt%)/ VC (8 wt%) that exhibited the value of 90 $Ah.kg^{-1}$ which is higher than the value of 70 $Ah.kg^{-1}$ of LMO/ Carbon Vulcan (10 wt%). These results suggested that the replacement of Carbon Vulcan by CNTs gave the efficiency of charge – discharge capacity due to high diffusion of lithium ions.

Similarly, the higher electrochemical performance was obtained for LMNO/CNTs (10 wt%) compared to the LMNO/Carbon Vulcan (10 wt%) which was shown in Figure 14. The high voltage of LNMO material exhibited

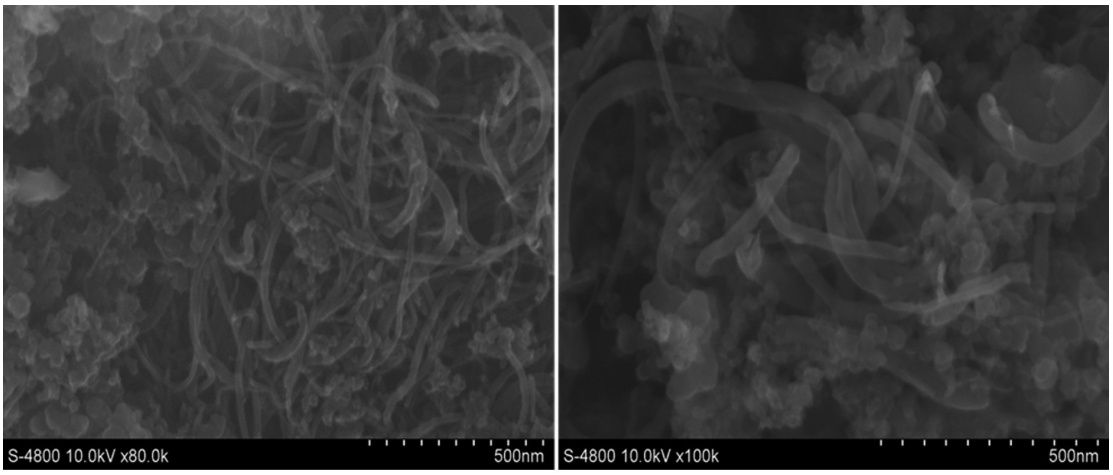

Figure 7. SEM images of LMO/CNTs (2 wt%) (a) and LNMO)/CNTs (2 wt%) (b) nanocomposites.

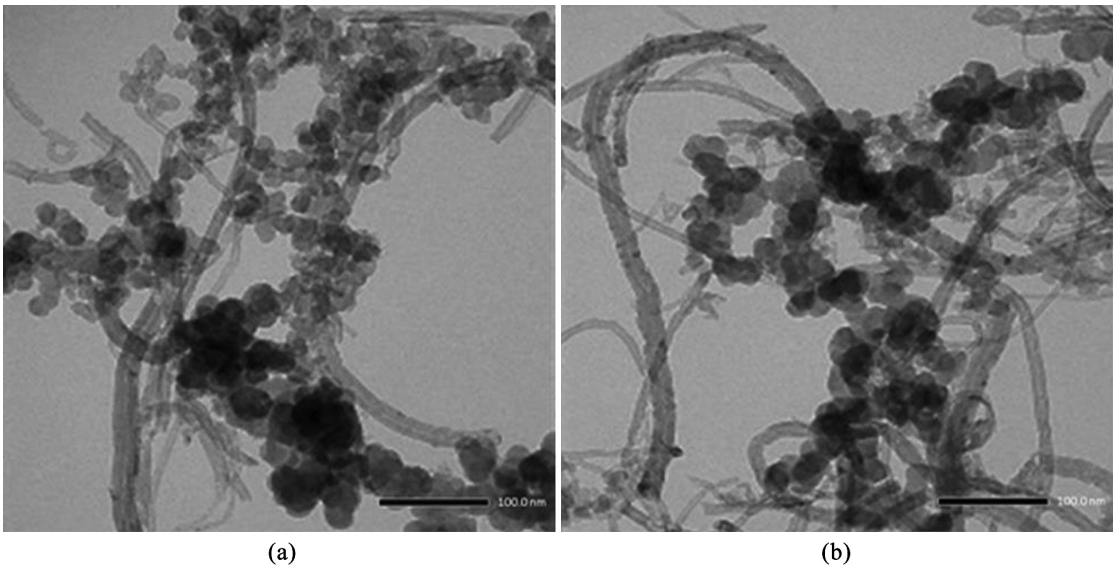

Figure 8. TEM images of LMO/CNTs (2 wt%) and LNMO/CNTs (2 wt%) nanocomposites.

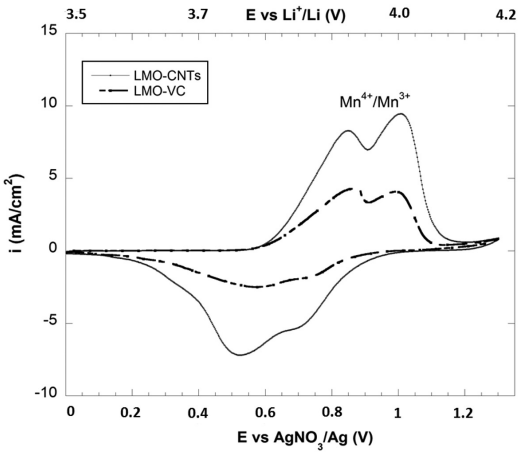

Figure 9. CV curves LMO/CNTs (2 wt%) nanocomposites (solid line) and LMO/VC (2 wt%) (dash dot line).

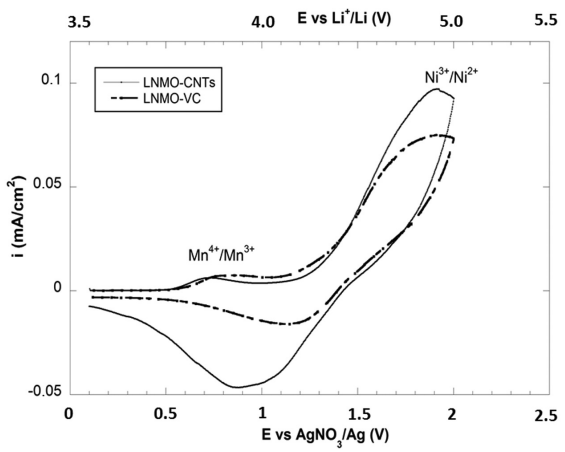

Figure 10. CV curves of LNMO/CNTs (2 wt%) nanocomposites (solid line) and LNMO/VC (2wt%) (dash dot line).

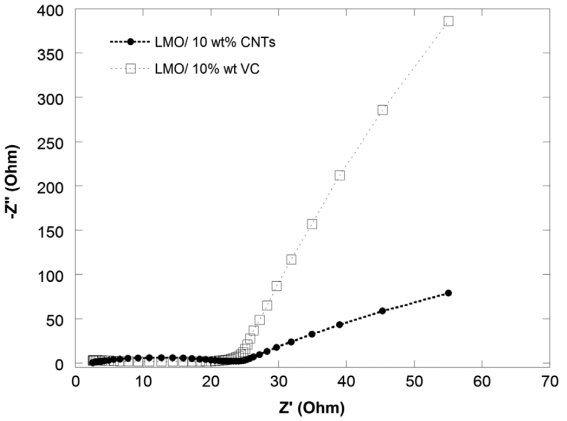

Figure 11. Nyquist plot of LMO/CNTs (10 wt%) nanocomposites (● plot) and LMO/Vulcan Carbon (10 wt%) (□ plot) composites electrode at room temperature.

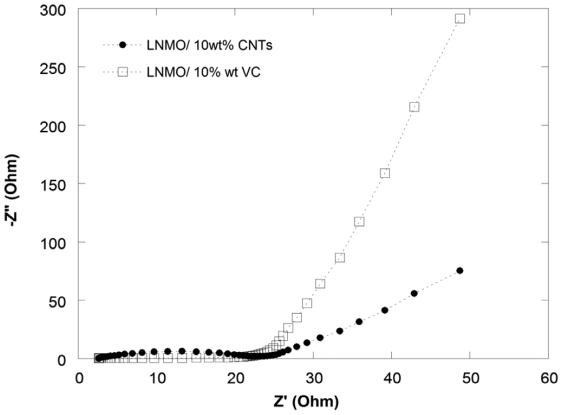

Figure 12. Nyquist plot of LNMO/CNTs (10 wt%) nanocomposite (● plot) and LNMO/Vulcan-Carbon (10 wt%) (□ plot) composite electrode at room temperature.

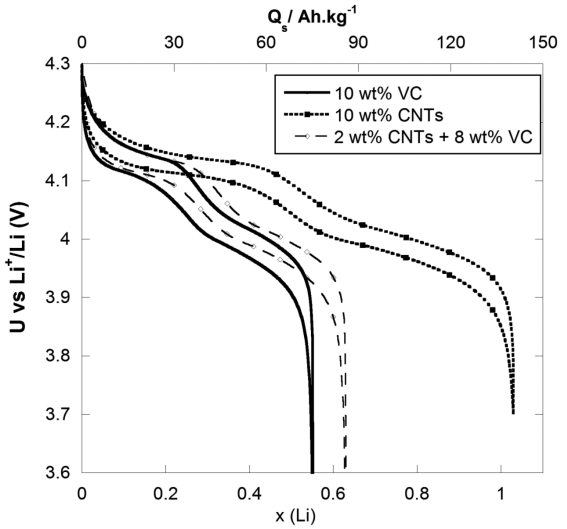

Figure 13. 1st charge discharge cycle at C/10 rate of nanocomposite electrodes: LMO/10 wt% VC, LMO/10 wt% CNT, LMO/2 wt% VC + 8 wt% VC.

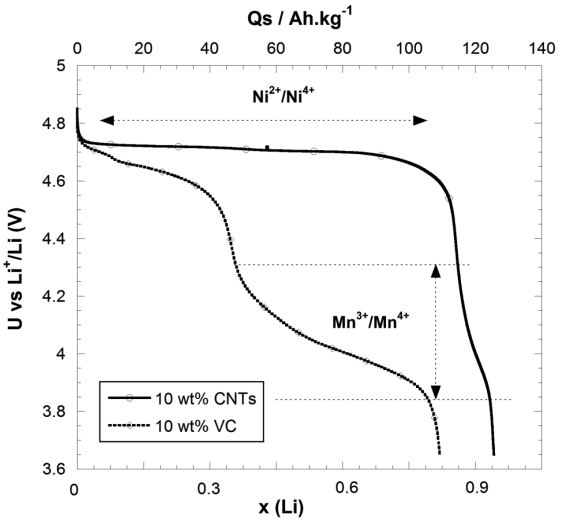

Figure 14. 1st charge discharge cycle at C/10 rate of nanocomposites electrodes: LNMO/VC (10 wt%) and LNMO/CNTs (10 wt%).

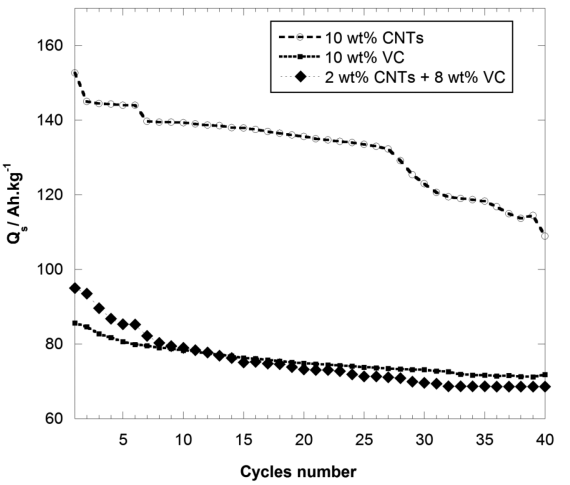

Figure 15. Cycling performance of nanocomposites electrodes at C/10 rate: LMO/VC (10 wt%), LMO/CNTs (2 wt%)/Carbon Vulcan (8 wt%) and LMO/CNTs (10 wt%).

principally the long plateaus at 4.75 V vs Li^+/Li and small shoulder at 4.2 V vs Li^+/Li.

The cycling performance of LMO (LNMO)/CNTs nanocomposites and LMO (LMNO)/ Carbon Vulcan was shown in Figure 15 and Figure 16 respectively. After 40 cycles, the capacity retentions were 80% for LMO/VC (10 wt%), 78% for LMO/CNTs (2 wt%)/Crabon Vulcan (8 wt%) and 75% for LMO/CNTs (10 wt%), respactively. These results proved that CNTs agent mixed in the composite electrode reduce slightly the cycle efficiency due to enhancement of Li^+ transport rate and electron into the spinel structure. It is well-known that LMO bulk material exhibited the poor cycle ability at the 4 voltage plateau because of Jahn – Teller distortion of the (MnO_6) octahedron caused by the Mn^{3+} cation at the 16d site[25]. The CNTs addition forming

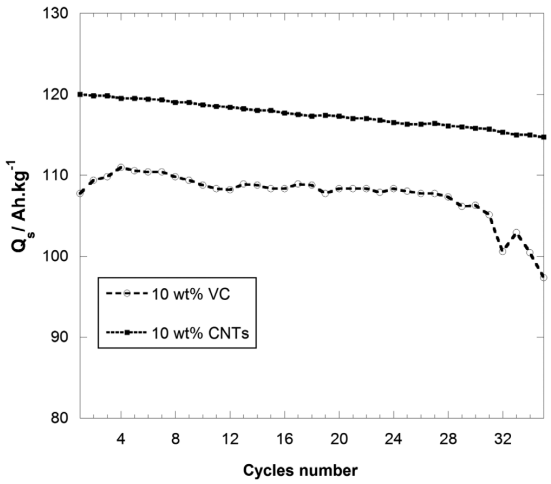

Figure 16. Cycling performance of nanocomposites electrodes at C/10 rate: LMO/10 wt% VC (10 wt%), LMO/CNTs (10 wt%), LMO/CNTs (2 wt%)/Carbon Vulcan (8 wt%).

the conducting network enhanced the electrical connections among $LiMn_2O_4$ particles therefore Li^+ intercalation/de-intercalation rate into/out of the spinel structure enhanced. In the other hand, the LNMO/CNTs (10 wt%) exhibited the excellent cycling behaviour in comparison with LNMO/VC (10 wt%). The capacity of LNMO/CNTs (10 wt%) remains 99% after 35 cycles. In fact, the Ni doped $LiMn_2O_4$ improved respectively the cyclability performance of $LiMn_2O_4$ due to the decrease of Mn^{3+}. Furthermore, LNMO exhibited the high voltage plateau at 4,75 V vs Li^+/Li corresponding to the oxidation couples of $Ni^{2+/}Ni^{4+}$.

5. Conclusion

We have successfully functionalized CNTs by a mixture of H_2SO_4/HNO_3. Addition, the LMO and LMNO nanoparticles were synthesized via solid state reaction. The electrode materials based on LMO/CNTs and LMNO/CNTs nanocomposites were prepared successfully by mixing process. The LMO/CNTs and LNMO/CNTs nanocomposites cathode materials have proved a remarkably higher efficiency of Mn^{3+}/Mn^{4+} and Ni^{2+}/Ni^{4+} redox couples in comparison to traditional cathodes based on LMO (LNMO)/Vulcan Carbon composite. Moreover the LMO/CNTs and LNMO/CNTs nanocomposites exhibited quiet high charge-discharge capacity as well as the stabilization of charge-discharge process. With this proof of concept, LMO/CNTs and LNMO/CNTs nanocomposites can act as promising cathode materials for development of high density and high power lithium rechargeable batteries.

Acknowledgements

This research was supported by The Department of Science and Technology (DOST) – Ho Chi Minh City. We would like to thank the supporting research of National Laboratory of Polymer and Composite Materials for helpful discussion.

References

1. Taberna PL, Mitra S, Poizot P, Simon P and Tarascon JM. High rate capabilities Fe_3O_4-based Cu nano-architectured electrodes for lithium-ion battery applications. *Nature Materials*. 2006; 5(7):567-573. http://dx.doi.org/10.1038/nmat1672. PMid:16783360.
2. Lu L, Wang JZ, Zhu XB, Gao XW and Liu HK. High capacity and high rate capability of nanostructured $CuFeO_2$ anode materials for lithium-ion batteries. *Journal of Power Sources*. 2011; 196(16):7025-7029. http://dx.doi.org/10.1016/j.jpowsour.2010.09.108.
3. Aricò AS, Bruce P, Scrosati B, Tarascon J-M and van Schalkwijk W. Nanostructured materials for advanced energy conversion and storage devices. *Nature Materials*. 2005; 4(5):366-377. http://dx.doi.org/10.1038/nmat1368. PMid:15867920.
4. Jiang C, Hosono E and Zhou H. Nanomaterials for lithium ion batteries. *Nano Today*. 2006; 1(4):28-33. http://dx.doi.org/10.1016/S1748-0132(06)70114-1.
5. Wallace GG, Chen J, Mozer AJ, Forsyth M, MacFarlane DR and Wang CY. Nanoelectrodes: energy conversion and storage. *Materials Today*. 2009; 12(6):20-27. http://dx.doi.org/10.1016/S1369-7021(09)70177-4.
6. Li H, Wang Z, Chen L and Huang X. Research on advanced materials for li-ion batteries. *Advanced Materials*. 2009; 21(45):4593-4607. http://dx.doi.org/10.1002/adma.200901710.
7. Chen J, Minett AI, Liu Y, Lynam C, Sherrell P, Wang C, et al. Direct growth of flexible carbon nanotube electrodes. *Advanced Materials*. 2008; 20(3):566-570. http://dx.doi.org/10.1002/adma.200701146.
8. Myung ST, Komaba S, Hirosaki NH, Yashiro H and Kumagai N. Emulsion drying synthesis of olivine $LiFePO_4$/C composite and its electrochemical properties as lithium intercalation material. *Electrochimica Acta*. 2004; 49(24):4213-4222. http://dx.doi.org/10.1016/j.electacta.2004.04.016.
9. Etacheri V, Marom R, Elazari R, Salitra G and Aurbach D. Challenges in the development of advanced Li-ion batteries: a review. *Energy & Environmental Science*. 2011; 4(9):3243-3262. http://dx.doi.org/10.1039/c1ee01598b.
10. Santhanagopalan S, Guo Q, Ramadass P and White RE. Review of models for predicting the cycling performance of lithium ion batteries. *Journal of Power Sources*. 2006; 156(2):620-628. http://dx.doi.org/10.1016/j.jpowsour.2005.05.070.
11. Doerffel D and Sharkh SA. A critical review of using the Peukert equation for determining the remaining capacity of lead-acid and lithium-ion batteries. *Journal of Power Sources*. 2006; 155(2):395-400. http://dx.doi.org/10.1016/j.jpowsour.2005.04.030.
12. Li X, Zhong Y, Cai M, Balogh MP, Wang D, Zhang Y, et al. Tin-alloy heterostructures encapsulated in amorphous carbon nanotubes as hybrid anodes in rechargeable lithium ion batteries. *Electrochimica Acta*. 2013; 89:387-393. http://dx.doi.org/10.1016/j.electacta.2012.11.097.
13. Tan L, Tang Q, Chen X, Hu A, Deng W, Yang Y, et al. Mesoporous LiFePO4 microspheres embedded homogeneously with 3D CNT conductive networks for enhanced electrochemical performance. *Electrochimica Acta*. 2014; 137:344-351. http://dx.doi.org/10.1016/j.electacta.2014.06.015.
14. Wang X, Sun L, Agung Susantyoko R, Fan Y and Zhang Q. Ultrahigh volumetric capacity lithium ion battery anodes with CNT–Si film. *Nano Energy*. 2014; 8:71-77. http://dx.doi.org/10.1016/j.nanoen.2014.05.020.

15. Bae SH, Karthikeyan K, Lee YS and Oh IK. Microwave self-assembly of 3D graphene-carbon nanotube-nickel nanostructure for high capacity anode material in lithium ion battery. *Carbon*. 2013; 64:527-536. http://dx.doi.org/10.1016/j.carbon.2013.08.003.

16. Liu XM, Huang ZD, Oh SW, Zhang B, Ma PC, Yuen MMF, et al. Carbon nanotube (CNT)-based composites as electrode material for rechargeable Li-ion batteries. *Composites Science and Technology*. 2012; 72(2):121-144. http://dx.doi.org/10.1016/j.compscitech.2011.11.019.

17. Li Z, Sun H, Xu J, Zhu Q, Chen W and Zakharova GS. The synthesis, characterization and electrochemical properties of V3O7·H2O/CNT Nanocomposite. *Solid State Ionics*. 2014; 262:30-34. http://dx.doi.org/10.1016/j.ssi.2013.09.002.

18. Abbas SM, Hussain ST, Ali S, Ahmad N, Ali N and Munawar KS. Synthesis of carbon nanotubes anchored with mesoporous Co_3O_4 nanoparticles as anode material for lithium-ion batteries. *Electrochimica Acta*. 2013; 105:481-486. http://dx.doi.org/10.1016/j.electacta.2013.04.179.

19. Mustansar Abbas S, Tajammul Hussain S, Ali S, Munawar KS, Ahmad N and Ali N. Facile synthesis of carbon nanotubes supported NiO nanocomposite and its high performance as lithium-ion battery anode. *Materials Letters*. 2013; 107:158-161. http://dx.doi.org/10.1016/j.matlet.2013.05.141.

20. Guo Q, Sun Z, Gao M, Tan Z, Zhang B and Su DS. Porous V_2O_5-SnO_2/CNTs composites as high performance cathode materials for lithium-ion batteries. *Journal of Energy Chemistry*. 2013; 22(2):347-355. http://dx.doi.org/10.1016/S2095-4956(13)60043-1.

21. Zhu XD, Tian J, Le SR, Chen JR and Sun KN. Enhanced electrochemical performances of $CuCrO_2$–CNTs nanocomposites anodes by in-situ hydrothermal synthesis for lithium ion batteries. *Materials Letters*. 2013; 107:147-149. http://dx.doi.org/10.1016/j.matlet.2013.05.137.

22. Pavlishchuk VV and Addison AW. Conversion constants for redox potentials measured versus different reference electrodes in acetonitrile solutions at 25°C. *Inorganica Chimica Acta*. 2000; 298(1):97-102. http://dx.doi.org/10.1016/S0020-1693(99)00407-7.

23. Hao YJ, Wang YY, Lai QY, Zhao Y, Chen LM and Ji XYJ. Study of capacitive properties for LT-$Li_4Mn_5O_{12}$ in hybrid supercapacitor. *Solid State Electrochem*. 2009; 13(6):905-912. http://dx.doi.org/10.1007/s10008-008-0627-y.

24. Arrebola JC, Caballero A, Hernán L and Morales J. A high energy Li-ion battery based on nanosized $LiNi_{0.5}Mn_{1.5}O_4$ cathode material. *Journal of Power Sources*. 2008; 183(1):310-315. http://dx.doi.org/10.1016/j.jpowsour.2008.04.036.

25. Arrebola JC, Caballero A, Gómez-Cámer JL, Hernán L, Morales J and Sánchez L. Combining 5 V $LiNi_{0.5}Mn_{1.5}O_4$ spinel and Si nanoparticles for advanced Li-ion batteries. *Electrochemistry Communications*. 2009; 11(5):1061-1064. http://dx.doi.org/10.1016/j.elecom.2009.03.014.